Acta Mech 206, 193–205 (2009)
DOI 10.1007/s00707-008-0098-3

L. Han · X. D. Wang · M. Zuo

The dynamic behavior of a surface-bonded piezoelectric actuator with a bonding layer

Received: 24 April 2008 / Accepted: 28 July 2008 / Published online: 9 October 2008

Abstract The performance of smart structures depends on the dynamic electromechanical behavior of piezoelectric actuators and the bonding condition along the interface, which connects the actuators and the host structures. This paper provides a theoretical study of the influence of material parameters of the bonding layer on the coupled electromechanical characteristics of piezoelectric actuators, which are subjected to high frequency electric loads. A one-dimensional actuator model with a bonding layer, which undergoes a shear deformation, is proposed. Analytical solutions based on the integral equation method are provided. Detailed numerical simulation is conducted to evaluate the effect of the bonding layer under different loading frequencies. The results indicate that the properties of the bonding layer, the loading frequency, the material combination and the geometry of the actuator have a significant effect on the load transfer between the actuator and the host medium.

1 Introduction

Piezoelectric materials with high electromechanical coupling properties have been widely used as sensors and actuators in structural health-monitoring (SHM) systems during the past few decades [1–5]. Compared with conventional transducers, piezoelectric sensors and actuators are small, thin and unobtrusive. They are low in cost and can be easily shaped and put into small spaces, or built inside of structures. Besides, they have high sensitivity to a wide range of loading frequencies, making them suitable for different dynamic applications.

The use of piezoelectric patches for damage detection of structures based on elastic wave propagation has attracted significant attention [6–8]. Elastic waves are sensitive to the changes of geometry and parameters of the material, and can propagate over a long distance in a structure. Therefore, they are attractive for the quick, large range inspection of structures. Extensive works have been done to study the use of piezoelectric patches as actuators and sensors for inducing and receiving elastic waves to conduct health monitoring of different structures [9–11].

The major difficulties in using elastic waves induced by piezoelectric actuators to conduct SHM are that the signals are not instinctually interpretable due to the complicated behavior of elastic waves, such as the dispersive characteristics of the waves, the presence of multi-modes, and the existence of complicated mode conversions [12,13]. These difficulties lead to further studies on the interaction between host structures and incorporated piezoelectric actuators, and the resulting complicated electromechanical behavior in a smart SHM system [14,15].

Because of the presence of material discontinuity between the actuators and the host structure, complicated local electromechanical fields are generated near the edges of the actuators. It is, therefore, necessary to have a clear understanding of the local stress field around piezoelectric actuators when they are used in structural

L. Han · X. D. Wang (✉) · M. Zuo
Department of Mechanical Engineering, University of Alberta, Edmonton, AB T6G 2G8, Canada
E-mail: xiaodong.wang@ualberta.ca

applications. A one dimensional actuator model was developed recently to study the static and dynamic electromechanical behavior of piezoceramic actuators attached to an elastic insulator when the system is subjected to in-plane mechanical and electrical loads [16]. Analytical and numerical studies are conducted to evaluate the effect of geometric and loading parameters upon the load transfer between the actuators and the host structure [17]. The interaction between different actuators is also studied by using a pseudo-incident wave method. This actuator model is also used to study the generation of Rayleigh waves for monitoring surface damage of structures using a single actuator and multiple actuators. This actuator model is further modified to study problems with varying electric field distribution along actuators [18].

In the above studies, however, the actuators are assumed to be perfectly bonded to the host structures, and the effect of the bonding layer is ignored. Since the modulus of the bonding layer is usually lower than that of the actuator and the host structures, it may significantly affect the local stress field distribution.

To study the influence of the bonding layer parameters on the active damping response of controlled beams, a bending-extensional dynamic model of a simply supported beam with attached piezoelements is proposed [19]. In this study, visco-elastic bonding layers, described by the Kelvin–Voigt model, are assumed. The results show that the stiffness of the bonding layer affects the active damping efficiency significantly. A three dimensional sensor model, which is later simplified into a two-dimensional one, is established to study the effect of the shear stress in the bonding layer on the sensing effectiveness of piezoelectric patches [20]. In this model, the bonding medium is considered as an elastic layer, with a finite stiffness in the thickness direction. This investigation shows that the strain drops sharply near the edges and the end-bonding must be carefully assessed to enhance the quality of the sensing output.

Unlike the cases of vibration control, in structural damage detection problems, high frequency elastic waves with wavelengths comparable to the size of the actuators are commonly generated inside the structures. The effects of the bonding condition on the dynamic behavior of the actuators in high frequency cases have not been studied thoroughly. Existing works in this area have been mostly limited to perfectly bonded actuators. It is, therefore, the objective of the current paper to provide a comprehensive theoretical study on the effects of the bonding layer on the dynamic behavior of piezoelectric actuators surface-bonded to an elastic substrate under high frequency loads. An integrated model containing a piezoelectric actuator, a viscoelastic bonding layer and an elastic medium (host) is proposed. Numerical simulation is conducted to simulate the effect of the geometric and material properties of the system, especially that of the bonding layer upon the coupled response of the actuators.

2 Formulation of the problem

Consider the problem of a thin piezoelectric actuator surface-bonded to a homogeneous and isotropic elastic insulator. Between the insulator and the actuator is a very thin visco-elastic bonding layer, as illustrated in Fig. 1. Plane strain deformation is assumed to simulate the case where the width of the sensor is large in comparison with its length. The dimension of the sensor is assumed significantly smaller than that of the host structure. Therefore, the host structure is modelled as a semi-infinite medium. The length of both the actuator and the bonding layer is denoted as $2a$, and the thickness of the actuator and the bonding layer is denoted as h and h', respectively. In Fig. 1, the z-axis is assumed to be along the poling direction of the actuator. The steady-state response of the system, including displacement, stress, and strain, will involve a time factor $\exp(-\mathrm{i}\omega t)$. For convenience, in the following discussion, this time factor will be suppressed and only the magnitudes of these field variables are used.

A voltage is applied between the upper and lower electrodes of the actuator, which results in an electric field of frequency ω along the poling direction of the actuator. The electric field intensity can be expressed as

$$E_z = (V^- - V^+)/h, \tag{1}$$

where V^- and V^+ represent the electric potential at the lower and upper surface of the actuator.

The present study is focusing on a thin-sheet actuator, with relatively small thickness in comparison with its length. Therefore, the applied electric field will mainly result in an axial deformation, $\varepsilon_y^{\mathrm{a}}$, where the superscript 'a' represents actuator. Consider the fact that the bonding layer is usually much thinner than the actuator; the axial stress and deformation are assumed to be uniform across the thickness of the bonding layer as well. The interfacial shear stress between different layers is denoted as τ, as shown in Fig. 2. u^+ and u^- in Fig. 2 represent the displacements on the upper and lower surface of the bonding layer, respectively.

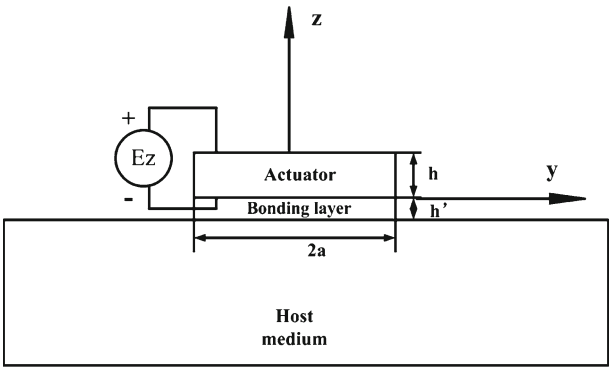

Fig. 1 Geometry of the system

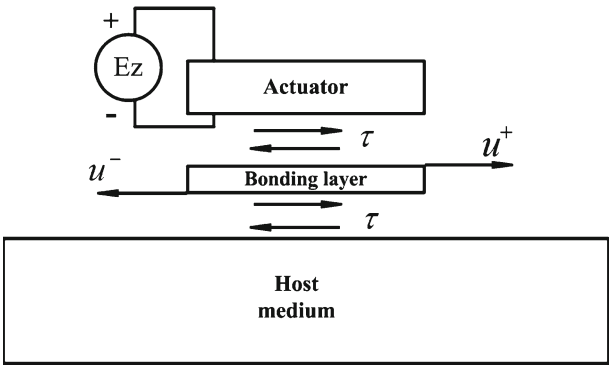

Fig. 2 Stress fields of the system

2.1 The bonding layer

The bonding layer is the connection between the actuator and the host structure. Its shear modulus, thickness, and coefficient of viscosity will determine the mechanical property of the layer.

The time-harmonic shear stress $\overline{\tau}$ distributed in the layer is determined by the constitutive relation

$$-\overline{\tau} = \mu_{\mathrm{b}}\overline{\varepsilon}_y + c_{\mathrm{b}}\dot{\overline{\varepsilon}}_y, \tag{2}$$

where

$$\overline{\tau} = \tau \exp(-\mathrm{i}\omega t), \tag{3}$$

$$\overline{\varepsilon}_y = \frac{u^+ - u^-}{h'} \exp(-\mathrm{i}\omega t), \tag{4}$$

$$\dot{\overline{\varepsilon}}_y = \frac{\partial\left[\left(\dfrac{u^+ - u^-}{h'}\right)\exp(-\mathrm{i}\omega t)\right]}{\partial t}, \tag{5}$$

with the subscript 'b' representing the bonding layer, μ_{b} and c_{b} being the shear modulus and the coefficient of viscosity of the bonding layer, respectively. τ is the magnitude of the shear stress distributed in the layer; $\overline{\varepsilon}_y$ is the longitudinal strain of the bonding layer; u^+ and u^- are the magnitudes of the longitudinal displacements of the upper and lower bonding layer surfaces, respectively.

Since u^+ and u^- are not functions of time, Eq. (2) can be rewritten as

$$-\tau = \left(\frac{\mu_\mathrm{b}}{h'} - \frac{\mathrm{i}\omega c_\mathrm{b}}{h'}\right)(u^+ - u^-). \tag{6}$$

This result is similar to the spring model used for interphases between two dissimilar media [21,22].

According to the continuity of the displacements, u^+ and u^- also denote the longitudinal displacements of the lower surface of the actuator and the upper surface of the host medium, respectively. Their expression can be obtained by analyzing the dynamic behavior of the actuator and the host medium.

2.2 Modelling of the actuator

For the case where the system is subjected to a high frequency electric field, the resulting wave propagation typically has a wave length comparable to the length of the actuator. Therefore, the inertia effect of the actuator must be considered [23] in the formulation of the actuator system. According to the thin-actuator assumption made, the equation of motion of the actuator can be expressed as

$$\frac{\mathrm{d}\sigma_y^\mathrm{a}}{\mathrm{d}y} + \tau(y)/h + \rho_a\omega^2 u_y^\mathrm{a} = 0, \tag{7}$$

where the superscript 'a' represents the actuator; σ_y^a, ρ_a, and u_y^a are the axial stress, the mass density and the axial displacement of the actuator, respectively.

As shown in [16,23,24], the axial stress of the actuator can be expressed as a function of the axial displacement u_y^a and the electric field E_z as

$$\sigma_y^\mathrm{a} = E_\mathrm{a}\frac{\partial u_y^\mathrm{a}}{\partial y} - e_\mathrm{a}E_z, \tag{8}$$

where E_a and e_a are effective material constants given in [16,23,24]. Since the two ends of the actuator are traction free, the following boundary condition should be satisfied:

$$\sigma_y^\mathrm{a} = 0, \quad |y| = a. \tag{9}$$

By substituting Eqs. (8) and (9) into Eq. (7), the longitudinal displacement of the actuator can be determined in terms of the shear stress τ as

$$u_y^\mathrm{a}(y) = f_\mathrm{E}(y) - \frac{\cos[k_\mathrm{a}(a+y)]}{k_\mathrm{a}E_\mathrm{a}\sin 2k_\mathrm{a}a}\int_{-a}^{a}\cos[k_\mathrm{a}(\xi-a)]p(\xi)\,\mathrm{d}\xi - \frac{1}{k_\mathrm{a}E_\mathrm{a}}\int_{-a}^{y}\sin[k_\mathrm{a}(y-\xi)]p(\xi)\,\mathrm{d}\xi \quad |y| < a, \tag{10}$$

where

$$f_\mathrm{E}(y) = \varepsilon_0\frac{\sin k_\mathrm{a}y}{k_\mathrm{a}\cos k_\mathrm{a}a} \tag{11}$$

is the axial displacement due to the applied electric field, and

$$p(y) = \frac{\tau(y)}{h}, \quad \varepsilon_0 = \frac{E_z e_\mathrm{a}}{E_\mathrm{a}}, \quad k_\mathrm{a} = \omega/c_\mathrm{a}, \quad c_\mathrm{a} = \sqrt{E_\mathrm{a}/\rho_\mathrm{a}} \tag{12}$$

with k_a and c_a being the wave number and wave speed of the actuator, respectively.

2.3 Dynamic behavior of the host medium

The dynamic plane strain displacement field in a homogeneous isotropic elastic medium is governed by [25],

$$u_y = \frac{\partial \Phi}{\partial y} + \frac{\partial \Psi}{\partial z}, \quad u_z = \frac{\partial \Phi}{\partial z} - \frac{\partial \Psi}{\partial y}, \tag{13}$$

where Φ and Ψ are two displacement potentials, which satisfy

$$(\nabla^2 + K^2)\Phi = 0, \quad (\nabla^2 + k^2)\Psi = 0, \tag{14}$$

in which the Laplace operator ∇^2 stands for $\frac{\partial^2}{\partial y^2} + \frac{\partial^2}{\partial z^2}$, and K and k are two wave numbers defined as

$$K = \omega/c_{\mathrm{L}}, \quad k = \omega/c_{\mathrm{T}} \tag{15}$$

with c_{L} and c_{T} being the longitudinal and transverse shear wave speed of the elastic medium, respectively.

Since there is no additional mechanical load applied to the host medium, the stress field generated inside the host structure is only due to the existence of the shear stress at its top surface caused by the actuator. The corresponding boundary conditions are

$$\begin{cases} \sigma_{yz}(y, 0) = -\tau & |y| < a, \\ \sigma_{yz}(y, 0) = 0 & |y| > a, \end{cases} \quad \sigma_z(y, 0) = 0. \tag{16}$$

The general solution of the wave induced by τ can be determined by solving the governing equations using the following Fourier transform:

$$f^*(s) = \frac{1}{2\pi} \int_{-\infty}^{\infty} f(y) e^{\mathrm{i}sy} \mathrm{d}y, \quad f(y) = \int_{-\infty}^{\infty} f^*(s) e^{-\mathrm{i}sy} \mathrm{d}s. \tag{17}$$

The general solution can be expressed as

$$\Phi^*(s, y) = A(s) e^{\alpha z}, \quad \Psi^*(s, y) = B(s) e^{\beta z} \tag{18}$$

from which the displacement components can be determined as

$$u_y^* = -\mathrm{i}sA(s) e^{\alpha z} + \beta B(s) e^{\beta z}, \tag{19}$$

$$u_z^* = \alpha A(s) e^{\alpha z} + \mathrm{i}sB(s) e^{\beta z}, \tag{20}$$

where $(^*)$ represents the Fourier transform. $A(s)$ and $B(s)$ are two unknown functions of s, and α and β are given by

$$\alpha = \begin{cases} \sqrt{s^2 - K^2} & |s| > K, \\ -\mathrm{i}\sqrt{K^2 - s^2} & |s| < K, \end{cases} \quad \beta = \begin{cases} \sqrt{s^2 - k^2} & |s| > k, \\ -\mathrm{i}\sqrt{k^2 - s^2} & |s| < k, \end{cases} \tag{21}$$

which ensure that the scattering stress field satisfies the radiation condition of the problem.

By making using of the general solution of u_y^* and u_z^* and the boundary conditions, the dynamic displacement along the interface between the bonding layer and the host medium can be determined as

$$u_y^{\mathrm{h}}(y, 0) = \frac{1}{\pi \mu_{\mathrm{h}}} \int_0^{\infty} \left(\frac{\beta k^2}{(2s^2 - k^2)^2 - 4s^2 \alpha \beta} + \frac{\lambda_0}{2s} \right) \int_{-a}^{a} \tau(\xi) \cos[s(y - \xi)] \, \mathrm{d}\xi \mathrm{d}s$$
$$+ \frac{\lambda_0}{2\pi \mu_{\mathrm{h}}} \int_{-a}^{y} \int_{-a}^{a} \tau(\xi) \frac{1}{y - \xi} \mathrm{d}\xi \mathrm{d}y, \quad |y| < a, \tag{22}$$

where the superscript and subscript 'h' represents the host medium, μ_{h} is the shear modulus of the matrix, and $\lambda_0 = 2(1 - \nu_{\mathrm{h}})$ with ν_{h} being the Poisson's ratio.

2.4 Dynamic load transfer

By substituting Eqs. (10) and (22) into Eq. (6), Eq. (6) can be rewritten as

$$
\begin{aligned}
&-\frac{\cos[k_{\mathrm{a}}(a+y)]}{k_{\mathrm{a}}E_{\mathrm{a}}\sin 2k_{\mathrm{a}}a}\int_{-a}^{a}\cos[k_{\mathrm{a}}(\xi-a)]p(\xi)\mathrm{d}\xi-\frac{1}{k_{\mathrm{a}}E_{\mathrm{a}}}\int_{-a}^{y}\sin[k_{\mathrm{a}}(y-\xi)]p(\xi)\mathrm{d}\xi\\
&-\frac{1}{\pi\mu_{\mathrm{h}}}\int_{0}^{\infty}\left[\frac{\beta k^2}{(2s^2-k^2)^2-4s^2\alpha\beta}+\frac{\lambda_0}{2s}\right]\int_{-a}^{a}\tau(\xi)\cos[s(y-\xi)]\mathrm{d}\xi\mathrm{d}s\\
&-\frac{\lambda_0}{2\pi\mu_h}\int_{-a}^{y}\int_{-a}^{a}\tau(\xi)\frac{1}{y-\xi}\mathrm{d}\xi\mathrm{d}y+\frac{h'}{\mu_{\mathrm{b}}-i\omega c_{\mathrm{b}}}\tau(y)=-f_{\mathrm{E}}(y),\quad |y|<a.
\end{aligned}
\tag{23}
$$

Equation (23) provides an integral equation in terms of the shear stress $\tau(y)$. To solve this equation, $\tau(y)$ will be expanded in terms of the first kind of Chebyshev polynomials, T_j, as

$$
\tau(y)=\sum_{j=0}^{\infty}c_jT_j(y/a)/\sqrt{1-y^2/a^2},
\tag{24}
$$

where

$$
T_j(y/a)=\cos(j\theta),\quad \cos\theta=y/a.
\tag{25}
$$

It should be mentioned that, in Eq. (23), the shear stress τ is not singular, since this equation represents displacements, which will always be bounded. The singularity involved in Eq. (24) is for mathematical reasons, i.e. simplifying the integral equation (23) and satisfying the orthogonality of Chebyshev polynomials. If τ is expanded to N terms, and Eq. (23) is satisfied at the following collocation points along the actuator

$$
y=a\cos\left[\frac{l}{N+1}\pi\right],\quad l=1,2,\ldots,N,\quad |y|<a
\tag{26}
$$

Equation (23) becomes N linear algebraic equations in terms of $\{c\}=\{c_0,c_1,\ldots,c_{N-1}\}^T$, the coefficients of Chebyshev expansion. These N equations can be written in the form

$$
[Q]\{c\}=\{F\},
\tag{27}
$$

where $[Q]$ is the resulting known matrix and $\{F\}$ is the applied load matrix, which are given in Appendix A.

By using Eq. (27), the coefficients of Chebyshev polynomials, $\{c\}$, can be obtained. It can then be used to determine the interfacial shear stress τ between the actuator and the host structure, by using Eq. (24).

3 Results and discussion

This section will be devoted to the discussion on the effects of different material, geometric and loading parameters on the load transfer from the actuator to the host structure, such as the material properties of the bonding layer, the material combination, the actuator geometries, and the loading frequency. A different material combination of the actuator and the host medium can be represented by the material mismatch factor q, which is defined as

$$
q=\frac{\pi E_{\mathrm{h}}}{2(1-\nu_{\mathrm{h}}^2)E_{\mathrm{a}}}.
\tag{28}
$$

The actuator geometry parameter, denoted as v, is defined as the ratio of the actuator length to its thickness:

$$
v=\frac{a}{h}.
\tag{29}
$$

Table 1 Material properties of the PZT actuator

Elastic stiffness parameters	c_{11}	c_{12}	c_{13}
(Pa)	13.9×10^{10}	6.78×10^{10}	7.43×10^{10}
Piezoelectric constants	e_{31}	e_{33}	e_{15}
(C m^{-2})	-5.2	15.1	12.7
Dielectric constants	λ_{11}	λ_{22}	λ_{33}
(C V^{-1} m^{-1})	6.45×10^{-9}	6.45×10^{-9}	5.62×10^{-9}

Table 2 Material properties of the host medium and the bonding layer

Host medium	
Young's modulus E_h (Pa)	5.2715×10^{10}
Poisson's ratio ν_h	0.3
Bonding layer	
Shear modulus μ_b (Pa)	1.0×10^9

The material constants of the piezoceramic (PZT) actuator are shown in Table 1 [26]. The material parameters of the host medium and the bonding layer are shown in Table 2. The material constant of the bonding layer is assumed based on existing material constants [27]. The Young's modulus of the host medium has been selected to result in a material mismatch parameter $q = \frac{\pi E_h}{2(1-\nu_h^2)E_a} = 1.0$. The mass densities of the actuator and the host medium, ρ_a and ρ_h, are assumed to be 2,700 kg/m^3. The loading frequency ka is selected ranging from 1.0 to 16.0, with $ka = 1.0$ corresponding to 0.09 MHz. The geometry of the actuator and the bonding layer are as follows: $a = 1$ cm, $h = 0.5$ mm ($v = 20$), and the range of h'/a is from 0 to 0.032.

3.1 Dynamic load transfer

The normalized interfacial shear stress $\tau^* = \tau/\sigma_B$, with $\sigma_B = qe_aE_z$, is an important indictor of the actuation efficiency, and represents the load transfer between the actuator and the host medium. In our discussion, the normalized interfacial shear stress will be used to investigate how different material parameters affect the load transfer from the actuator to host medium.

3.1.1 The effect of the thickness of the bonding layer

As indicated in Eq. (6), the mechanical property of the bonding layer is governed by its stiffness μ_b/h'. In the following discussion, μ_b is set to be a constant value, and only the value of h' is changed to obtain different stiffness of the bonding layer.

To investigate the load transfer between the actuator and the host medium, different thicknesses, $h' = 0$, 10, 40, 80, 160 and 320 μm, are selected to study how the normalized interfacial shear stress varies with the increase of the thickness of the bonding layer, when the system is subjected to electric fields with different loading frequencies.

Figure 3 shows the shear stress distribution for the case where the loading frequency is $ka = 1.0$ and $c_b = 0.0$ for different thickness of the bonding layer. Comparing the six curves in this figure, it can be clearly seen that, as the h' value increases from 0 to 320 μm, the shear stress level along the actuator in the interval of $y/a = 0$–0.9 shows very limited variation, but the stress concentration at the tip of the actuator, $y/a = 1.0$, decreases significantly.

The corresponding results for a higher frequency $ka = 4.0$ are displayed in Fig. 4. Similarly, more significant stress concentration is observed when the thickness of the bonding layer decreases, but in this case, with the increase of h', a dramatic change in shear stress distribution along the actuator is observed. When h' is between 0 and 160 μm, the shear stress increases, approaching the tip of the actuator. However, when $h' = 320$ μm, the shear stress value decreases in the interval of $y/a = 0.6$–1.0. Figure 5 shows a very similar phenomenon for the case where $ka = 8.0$. When h' goes up to 160 and 320 μm, the stress value decreases as y/a increases from 0.8 to 1.0. These results indicate that with the increase of the thickness of the layer, the

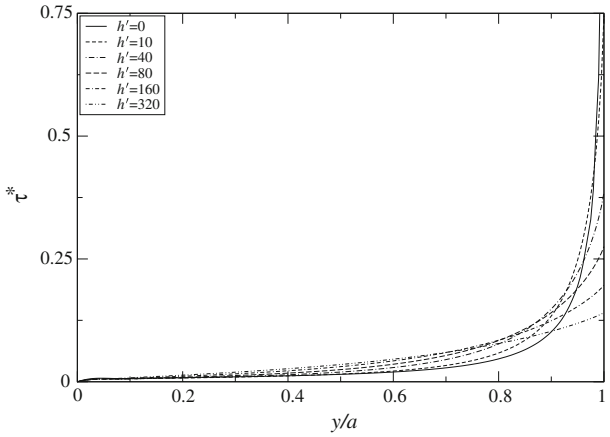

Fig. 3 Normalized shear stress distribution along the actuator with different thicknesses of the bonding layer ($ka = 1.0$, $q = 1.0$, $v = 20.0$)

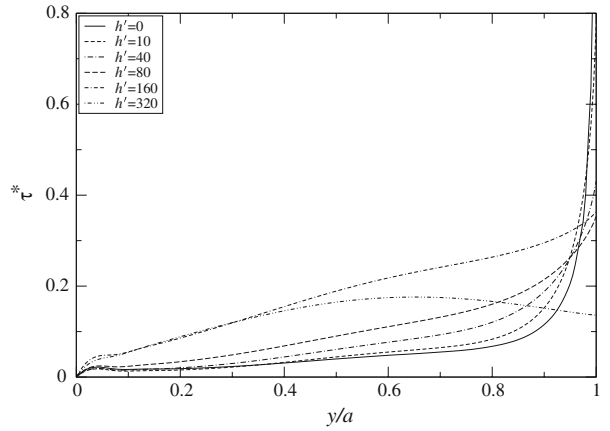

Fig. 4 Normalized shear stress distribution along the actuator with different thicknesses of the bonding layer ($ka = 4.0$, $q = 1.0$, $v = 20.0$)

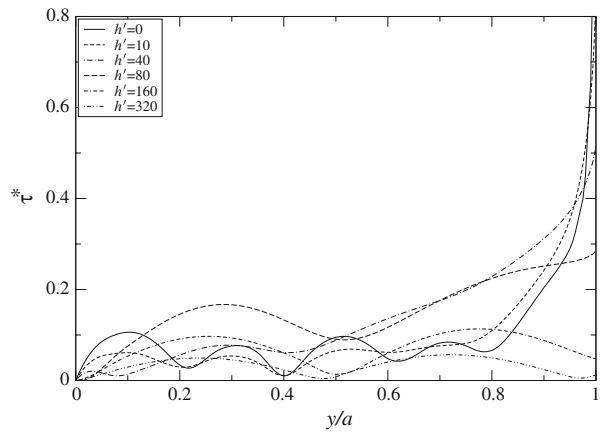

Fig. 5 Normalized shear stress distribution along the actuator with different thicknesses of the bonding layer ($ka = 8.0$, $q = 1.0$, $v = 20.0$)

shear stress concentration near the tip of the actuator becomes less important. With the increase of the loading frequency, the effect of the thickness of the bonding layer on the load transfer between the actuator and the host medium becomes more and more significant, not only at the tip of the actuator.

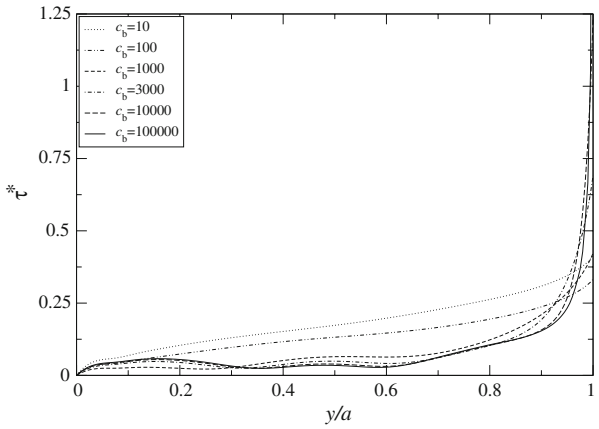

Fig. 6 Normalized shear stress distribution with different coefficients of viscosity ($ka = 5.0$, $h' = 100$, $q = 1.0$, $v = 20.0$)

3.1.2 The effect of the coefficient of viscosity

The coefficient of viscosity of the bonding layer also affects the load transfer between the actuator and the host medium, although its effect may not be as significant as that of the thickness or the modulus of the layer. For the case where $ka = 5.0$ (corresponding to 0.45 MHz) and $h' = 100$ μm, different coefficients of viscosity of the bonding layer, $c_b = 10{,}100$, 1,000, 3,000, 10,000 and 100,000 Pa s, are selected. The corresponding distribution of the normalized shear stress along the actuator is shown in Fig. 6.

Since in this case the thickness of the layer is quite significant, the shear stress concentration near the tip of the actuator is not obvious for a low coefficient of viscosity ($c_b = 10$–100 Pa s). As c_b increases, a higher concentration of the shear stress around the tip of the actuator is observed. For high c_b value ($c_b = 100{,}000$ Pa s), the stress concentration around the tip becomes very significant. In fact, the stiffness of the bonding layer is increased with increasing c_b. When c_b is very high, the property of the layer is close to that under the perfect bonding conditions.

3.1.3 The effect of the loading frequency

The significant effect of the loading frequency upon the shear stress distribution has been observed by comparing the results shown in Figs. 3, 4, and 5. To evaluate the effect of the loading frequency in detail, a series of frequencies, $ka = 1.0$, 2.0, 4.0, 8.0, and 16.0, are selected in the following examples under two bonding conditions, $h' = 0$ and $h' = 100$ μm with $c_b = 0$.

The normalized shear stress distribution for perfectly bonded actuator ($h' = 0$) is depicted in Fig. 7 for different loading frequencies. The results for the corresponding cases with a bonding layer ($h' = 100$ μm) are given in Fig. 8.

In Fig. 7, the increase of the loading frequency results in an increase of the shear stress away from the tip of the actuator. A similar phenomenon is observed in Fig. 8, where a bonding layer is included. However, with the increase of the loading frequency, the singular behavior of the shear stress at the tip of the actuator becomes less obvious.

3.1.4 The effect of the material mismatch

The material mismatch parameter $q = \frac{\pi E_h}{2(1-\nu_h^2)E_a}$ is an indicator of the relative modulus of the actuator to the host medium. For the current selection of the materials of the actuator, the bonding layer and the host medium as given in Tables 1 and 2, $q = 1.0$. To study the effect of material mismatch q, the material constants of the actuator are fixed, and the shear modulus of the host medium is changed to achieve different material combinations. In this section, $q = 0.1$, 0.5, 1.0, 2.0 and 5.0 are chosen, and two bonding conditions, $h' = 0$ and $h' = 100$ μm, are considered to investigate the effect of material combinations on the load transfer between the actuator and the host structure. The loading frequency is selected to be $ka = 5.0$, and the normalized shear stress distribution curves under these two bonding conditions are shown in Figs. 9 and 10, respectively.

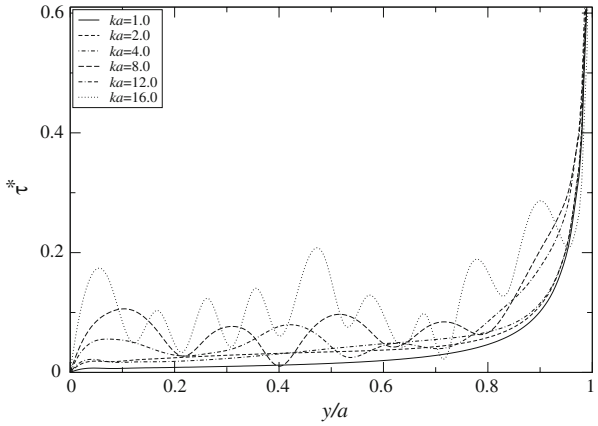

Fig. 7 Normalized shear stress distribution with different loading frequencies ($h' = 0$, $q = 1.0$, $v = 20.0$)

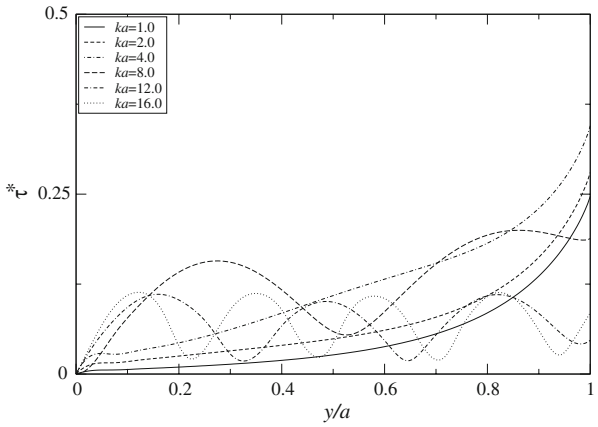

Fig. 8 Normalized shear stress distribution with different loading frequencies ($h' = 100$, $q = 1.0$, $v = 20.0$)

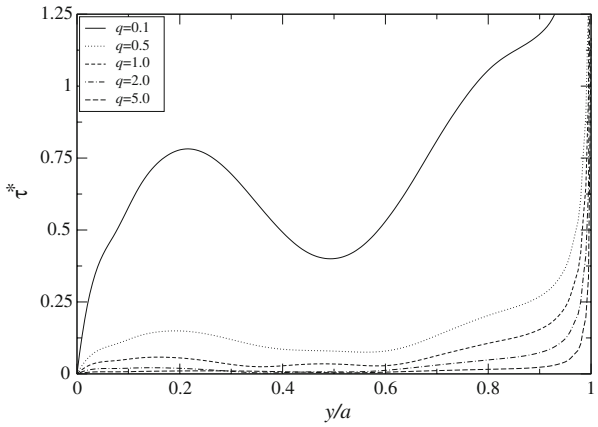

Fig. 9 Normalized shear stress distribution along the actuator with different material combinations ($ka = 5.0$, $h' = 0$, $v = 20.0$)

In Fig. 9, with the decrease of q, an increase of the shear stress level can be observed. When q approaches 0.1, corresponding to a stiff actuator, a significant increase in the shear stress along the actuator is observed.

Figure 10 shows very similar results, which is for the case where the bonding layer is included. In this case, the singular behavior of the shear stress at the tip of the actuator is significantly reduced. This result indicates the coupled effect of the material mismatch and the bonding layer property upon the load transfer. Proper selection of material combination, if possible, could increase the actuation efficiency of the actuator.

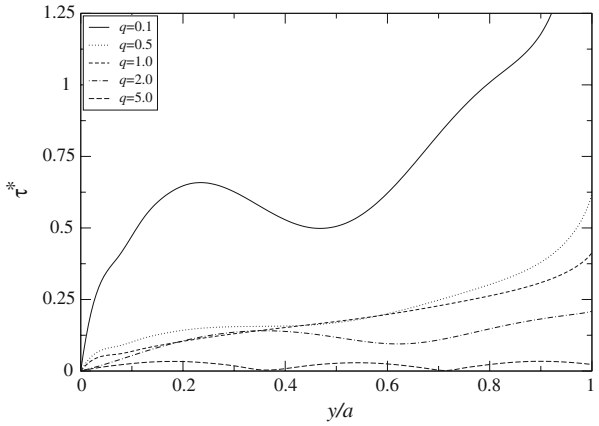

Fig. 10 Normalized shear stress distribution along the actuator with different material combinations ($ka = 5.0$, $h' = 100$, $v = 20.0$)

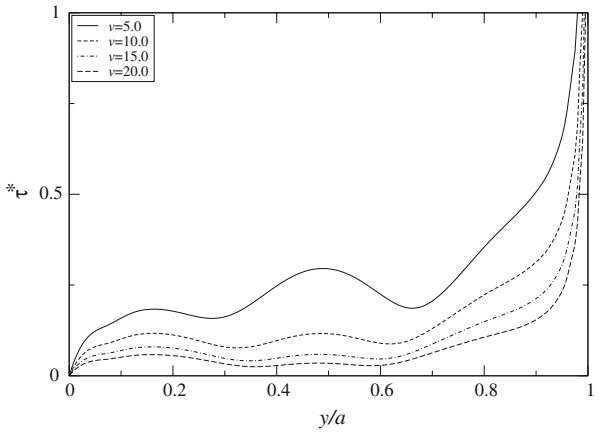

Fig. 11 Normalized shear stress distribution with different actuator geometries ($ka = 5.0$, $h' = 0$, $q = 1.0$)

3.1.5 The effect of the geometry of the actuator

The effect of the geometry of the actuator upon the load transfer between the actuator and the host medium is also studied. The actuator geometry is represented by the ratio of its length to its thickness, $v = a/h$. Four v values, $v = 5.0$, 10.0, 15.0, and 20.0, are selected to evaluate this effect. $ka = 5.0$ is chosen as the loading frequency, and two bonding conditions, $h' = 0$ and $h' = 100$ μm are considered. The results with $h' = 0$ and $h' = 100$ μm are displayed in Figs. 11 and 12, respectively.

As shown in Fig. 11, the decrease in the v value makes shear stress distribution less concentrated around the tip of the actuator. Increase of shear stress level along the actuator due to decreasing v is also observed.

When a bonding layer is included, as shown in Fig. 12, the stress concentration around the tip of the actuator is dramatically reduced in comparison with the corresponding curve in Fig. 11. It is also observed that the shear stress distribution along the actuator has also been significantly affected in comparison with the result given in Fig. 11.

4 Concluding remarks

This paper studies the effect of different material and geometric parameters of the bonding layer and the actuator on the load transfer from the actuator to the host medium, when a high frequency electric field is applied to the actuator. An analytical solution is provided, and numerical simulation is conducted for special cases. The current results indicate that, for relatively low frequency cases, the increase of the bonding layer thickness will increase the shear stress level along the internal surface of the actuator, and decrease the stress

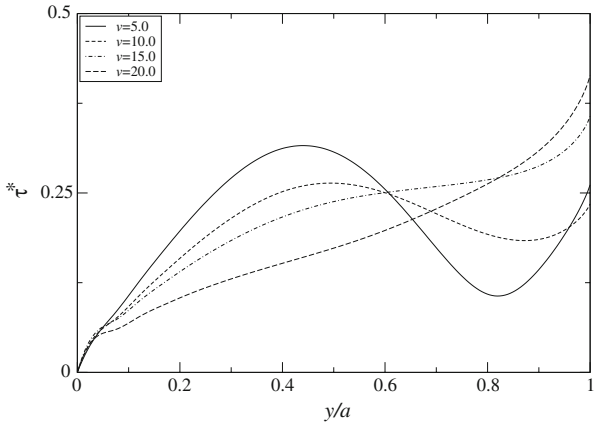

Fig. 12 Normalized shear stress distribution with different actuator geometries ($ka = 5.0$, $h' = 100$, $q = 1.0$)

concentration at the tips of the actuator. For relatively high frequency cases, however, the increase of the bonding layer thickness results in a shear stress distribution curve along the actuator varying significantly from that obtained by a perfectly bonded actuator, both in shape and amplitude. Therefore, for using the currently selected actuator to induce elastic waves in the host structure, the loading frequency of the electric field should not be too high ($ka < 5.0$, for example). In addition, the material combination and actuator geometry show more significant influence on the shear stress distribution when a bonding layer is included.

Appendix: Actuator solution

The matrix $[Q]$ used in Eq. (27) is given by

$$
\begin{aligned}
Q_{lj} = & -\pi \frac{\cos[\overline{k}_{\mathrm{a}}(1+\eta^l)]}{\overline{k}_{\mathrm{a}} E_{\mathrm{a}} \overline{h} \sin(2\overline{k}_{\mathrm{a}})} P_j^2 \\
& + \frac{1}{\overline{k}_{\mathrm{a}} E_{\mathrm{a}} \overline{h}} \int_{\cos^{-1}\eta^l}^{\pi} \sin\left[\overline{k}_{\mathrm{a}}(\cos\theta - \eta^l)\right] \cos(j\theta)\mathrm{d}\theta \\
& - \frac{1}{\mu_h} \int_0^{\infty} P_j^1 \left(\frac{\overline{\beta k}^2}{[(2\overline{s}^2 - \overline{k}^2)^2 - 4\overline{s}^2 \overline{\alpha}\overline{\beta}]} + \frac{\lambda_0}{2\overline{s}} \right) \mathrm{d}\overline{s} + \frac{\lambda_0}{2\mu_{\mathrm{h}}} P_j^3 + \frac{\overline{h'}}{(\mu_{\mathrm{b}} - \mathrm{i}\omega c_{\mathrm{b}})} \cdot \frac{T_j(\eta^l)}{\sqrt{1-\eta^{l2}}},
\end{aligned}
$$

where

$$
\eta^l = y^l/a, \quad \overline{k} = ka, \quad \overline{k}_{\mathrm{a}} = k_{\mathrm{a}} a, \quad \overline{s} = sa
$$

and

$$
\left.
\begin{aligned}
P_j^1 &= J_j(\overline{s}) \begin{cases} (-1)^n \sin(\overline{s}\eta^l) & j = 2n+1 \\ (-1)^n \cos(\overline{s}\eta^l) & j = 2n \end{cases} \\
P_j^2 &= J_j(\overline{k}_{\mathrm{a}}) \begin{cases} (-1)^n \sin(\overline{k}_{\mathrm{a}}) & j = 2n+1 \\ (-1)^n \cos(\overline{k}_{\mathrm{a}}) & j = 2n \end{cases} \\
P_j^3 &= \begin{cases} \frac{[\cos(j\cos^{-1}\eta^l) - (-1)^j]}{j} & j \neq 0 \\ 0 & j = 0 \end{cases}
\end{aligned}
\right\}
$$

with J_j ($j = 1, 2, \ldots$) and T_j being the Bessel functions of the first kind and the Chebyshev polynomials, respectively.

$\overline{\alpha}$, $\overline{\beta}$ can be obtained from α, β directly, with s and k being replaced by $\overline{s}$ and $\overline{k}$, respectively.

The loading matrix $\{F\}$ used in Eq. (27) is given by

$$\{F\} = \frac{f_{\mathrm{E}}(\eta^l)}{a} = \varepsilon_0 \frac{\sin \bar{k}_{\mathrm{a}} \eta^l}{\bar{k}_{\mathrm{a}} \cos \bar{k}_{\mathrm{a}}}. \tag{30}$$

References

1. Gandhi, M.V., Thompson, B.S.: Smart Materials and Structures. Chapman Hall, London (1992)
2. Banks, H.T., Smith, R.C., Wang, Y.: Smart Material Structures: Modelling, Estimation and Control. Masson, John Wiley and Sons, Paris (1996)
3. Chee, C., Tong, L., Steven, G.P.: A review on the modeling of piezoelectric sensors and actuators incorporated in intelligent structures. J. Intell. Mater. Syst. Struct. **9**, 3–19 (1998)
4. Cohen, Y.B.: Emerging NDE technologies and challenges at the beginning of the 3rd millennium-part I. Mater. Eval. **58**(1), 17–30 (2000)
5. Boller, C.: Next generation structural health monitoring and its integration into aircraft design. International Journal of Systems Science **31**, 1333–1349 (2000)
6. Chang, F.K.: Built-in damage diagnostics for composite structures. In: Proceedings of the 10th International Conference on Composite Structures (ICCM-10), vol. 5, pp. 283–289 (1995)
7. Lin, X., Yuan, F.G.: Pre-stack reverse time migration in structural health monitoring. In: 41st AIAA/ASME/ASCE/AHS/ASc Structures, Structural Dynamics and Materials Conference and Exhibit, Atlanta, 1984–1994 (2000)
8. Park, J.M., Kong, J.W., Kim, D.S., Yoon, D.J.: Nondestructive damage detection and interfacial evaluation of single-fibers/epoxy composites using PZT, PVDF and P(VDF-TrFE) copolymer sensors. Compos. Sci. Technol. **65**(2), 241–256 (2005)
9. Gibbs, G.P., Fuller, C.R.: Excitation of thin beams using asymmetric piezoelectric actuators. J. Acoust. Soc. Am. **92**, 3221–3227 (1992)
10. Tracy, M., Chang, F.K.: Identifying impacts in composite plates with piezoelectric strain sensors. Part I. Theory. J. Intell. Mater. Syst. Struct. **9**(11), 920–928 (1998)
11. Lestari, W., Qiao, P.Z.: Application of wave propagation analysis for damage identification in composite laminated beams. J. Compos. Mater. **39**(22), 1967–1984 (2005)
12. Alleyne, D.N., Cawley, P.: Optimization of Lamb wave inspection techniques. NDT and E Int. **25**(1), 11–22 (1992)
13. Jin, J., Quek, S.T., Wang, Q.: Wave boundary element to study Lamb wave propagation in plates. J. Sound Vib. **288**, 195–213 (2005)
14. Wang, B.L., Mai, Y.W.: Fracture of a piezoelectric material layer bonded by two elastic layers. Int. J. Eng. Sci. **40**(15), 1697–1727 (2002)
15. Zhang, B., Zhang, J.: Electromechanical interaction behaviors of piezoelectric sensor and actuator on elastic substrate. J. Intell. Mater. Syst. Struct. **16**(7–8), 589–595 (2005)
16. Wang, X.D.: Coupled electromechanical behavior of piezoelectric actuators in smart structures. J. Intell. Mater. Syst. Struct. **10**(3), 232–241 (1999)
17. Wang, X.D., Huang, G.L.: Wave propagation in electromechanical structures: induced by surface bonded piezoelectric actuators. J. Intell. Mater. Syst. Struct. **12**(2), 105–115 (2001)
18. Wang, X.D., Huang, G.L.: Wave propagation generated by piezoelectric actuators attached to elastic substrates. Acta Mech. **183**, 155–176 (2006)
19. Pietrzakowski, M.: Active damping of beams by piezoelectric system: Effects of bonding layer properties. Solids Struct. **38**, 7885–7897 (2001)
20. de Faria, A.R.: The impact of finite stiffness bonding on the sensing effectiveness of piezoelectric patches. Smart Mater. Struct. **12**, N5–N8 (2003)
21. Yang, J.S., Hu, Y.T., Zeng, Y., Fan, H.: Thickness-shear vibrations of rotated Y-cut quartz plates with imperfectly bonded surface mass layers. IEEE Trans. Ultrasonics Ferroelectr. Freq. Control **53**, 241–245 (2006)
22. Handge, U.A.: Analysis of a shear-lag model with nonlinear elastic stress transfer for sequential cracking of polymer coatings. J. Mater. Sci. **37**, 4775–4782 (2002)
23. Wang, X.D., Huang, G.L.: The coupled dynamic behavior of piezoelectric sensors bonded to elastic media. J. Intell. Mater. Syst. Struct. **17**, 883–894 (2006)
24. Yang, J.S.: Equations for the flexural motion of elastic plates with partially electroded piezoelectric actuators. Smart Mater. Struct. **6**, 485–490 (1997)
25. Achenbach, J.D.: Wave Propagation in Elastic Solids. North-Holland, Amsterdam (1973)
26. Park, Y.E.: Crack extension force in a piezoelectric material. ASME J. Appl. Mech. **57**, 647–653 (1990)
27. Park, J.M., Kim, D.S., Han, S.B.: Properties of interfacial adhesion for vibration controllability of composite materials as smart structures. Compos. Sci. Technol. **60**, 1953–1963 (2000)